Structural reinforcement and failure analysis in composite nanofibers of graphene oxide and gelatin

CrossMark

Silvia Panzavolta [a,*], Barbara Bracci [a], Chiara Gualandi [a], Maria Letizia Focarete [a], Emanuele Treossi [b,c], Konstantinos Kouroupis-Agalou [b,c], Katia Rubini [a], Federico Bosia [d], Lucas Brely [d], Nicola M. Pugno [e,f,g], Vincenzo Palermo [b,c,*], Adriana Bigi [a]

[a] Department of Chemistry "Giacomo Ciamician", University of Bologna, Via Selmi, 2, 40126 Bologna, Italy
[b] ISOF – Istituto per la Sintesi Organica e la Fotoreattività, Consiglio Nazionale delle Ricerche, via Gobetti 101, 40129 Bologna, Italy
[c] Laboratorio MIST.E-R Bologna, via Gobetti 101, 40129 Bologna, Italy
[d] Department of Physics and "Nanostructured Interfaces and Surfaces" Centre, Università di Torino, Via P. Giuria 1, 10125 Torino, Italy
[e] Laboratory of Bio-Inspired & Graphene Nanomechanics, Department of Civil, Environmental and Mechanical Engineering, Università di Trento, via Mesiano, 77, I-38123 Trento, Italy
[f] Center for Materials and Microsystems, Fondazione Bruno Kessler, Via Sommarive 18, I-38123 Povo (Trento), Italy
[g] School of Engineering and Materials Science, Queen Mary University of London, Mile End Road, London E1 4NS, United Kingdom

ARTICLE INFO

ABSTRACT

In this work we study the mechanical properties and failure mechanism of nanocomposites of graphene oxide sheets embedded in polymeric systems, namely films and electro-spun nanofibers. In this last system, contrary to conventional bulk composites, the size of the nano-reinforcement (GO sheets) is comparable to the size of the nanofibers to be reinforced ($\approx$ 200 nm). As polymeric matrix we use gelatin. We demonstrate that the high chemical affinity of the two materials hinders the renaturation of gelatin into collagen and causes a nearly ideal mixing in the GO–gelatin composite. Adding just 1% of GO (wt of GO with respect to gelatin) we obtain an increase of Young's modulus >50% and an increase of fracture stress >60%. We use numerical simulations to study the failure mechanism of the fibers. Calculations well agree with experimental data and show that, even if cracks start at GO sheet edges due to stress concentrations, crack propagation is hindered by the nonlinear behaviour of the matrix. Moreover, the presence of the GO sheets in continuous gelatin films improves the material stability to phosphate buffer solutions from 2 days to 2 weeks, making it a better material than gelatin for applications in biological environments.

1. Introduction

Nanofiller/polymer composites find a wide range of applications, thanks to the ability of the nanofiller to improve the mechanical, chemical, thermal and optical properties of the matrix [1,2].

Among nano-fillers, the newest and most studied class of materials is that of so-called 2-dimensional materials, such as

---

* *Corresponding authors:* Address: ISOF – Istituto per la Sintesi Organica e la Fotoreattività, Consiglio Nazionale delle Ricerche, via Gobetti 101, 40129 Bologna, Italy (V. Palermo), Department of Chemistry "Giacomo Ciamician", University of Bologna, Via Selmi, 2, 40126 Bologna, Italy (S. Panzavolta)
E-mail addresses: silvia.panzavolta@unibo.it (S. Panzavolta), palermo@isof.cnr.it (V. Palermo).

graphene and its derivatives [3]. While graphene can improve the mechanical, electrical and thermal properties of composites, its efficient processing and interaction with the polymer matrix is still problematic. The role of graphene as mechanical reinforcement can become all the more useful in biomaterials that have usually very poor mechanical properties or stability.

A widely used biomaterial is gelatin. Gelatin has attracted great interest due to its peculiar properties. This biopolymer is obtained by chemical or thermal degradation of collagen, which causes the rupture of the collagen triple helix into the random-coil structure characteristic of gelatin. The sol–gel transformation that takes place on cooling gelatin aqueous solutions is a conformational disorder–order transition of the gelatin chains that results in a partial regeneration of the triple helix structure [4–6]. The stiffness of gelatin gels and the mechanical properties of drawn gelatin films have been related to the renaturation level, that is the triple helix content of the protein [5–8]. Gelatin is cheaper than collagen and it does not express antigenicity in physiological conditions [9,10]. In addition, gelatin is biodegradable and biocompatible, which justifies its numerous uses in the pharmaceutical and medical fields for a variety of applications, including tissue engineering, wound dressing, drug delivery and gene therapy [11]. Moreover, gelatin-based films are thin, flexible and transparent materials widely employed in engineering food, packaging and drug recover [12,13]. However, the main drawback in the use of gelatin is related to its poor mechanical properties, which limit its range of application. The mechanical performance of the biopolymer can be improved through reinforcement with fillers. A variety of materials, including carbon fibers, clay, hydroxyapatite, have been proposed to this aim [2,14,15]. Recently, it was reported that reinforcement with graphene oxide nanoplatelets induced remarkable improvement of gelatin films mechanical properties [16].

Graphene oxide (GO) can be obtained in large quantities by chemical oxidation of graphite and processed efficiently in different solvents as single sheets with lateral size tunable from 100 μm to 100 nm, and with a nearly 100% yield of monolayers [17,18]; Furthermore, GO can be functionalized in different ways to enhance its interaction with other molecules and with the surrounding environment [19,20], displaying high Young's modulus, hardness and flexibility [21]. Whilst the positive effect of GO nano-fillers has been proved for different composite systems [22–24] there is less evidence on what the exact failure mechanism is in these composite materials at the nanoscale [25].

In this paper, we study the mechanical properties and failure mechanism of nano-composites made of graphene oxide sheets and gelatin. We do not limit the study to bulk composite layers, but also prepare and characterize more challenging systems in which the composite is electrospun in nano-fibers.

In these systems, contrary to conventional bulk composites, the size of the nano-reinforcement (GO sheets) is comparable to the size of the nanofibers to be reinforced (≈200 nm). The electrospinning production method itself is challenging, because the fibers undergo significant mechanical and electrical stress during spinning; only highly stable and defect-free composites can be processed in this way.

Continuous electrospun nanofibers are becoming increasingly of interest in the field of functional and structural materials [26] as well as in the biomedical sector [27] due to high open porosity of the nanofibers assemblies, associated to their remarkable specific surface area and extreme flexibility. The first attempt to produce polymeric electrospun nanofibres filled with GO dates back to 2010 [28]. Very recently polymers with polar groups, thus capable of interacting with oxygen-containing hydrophilic groups located at the surface of GO – such as poly(vinyl alcohol) [29], poly(acrylonitrile) [30–32] and poly(amides) [33] – have been electrospun with GO obtaining mats with remarkably improved mechanical properties. No attempt to prepare electrospun gelatin nanofibers enriched with GO has been reported up to now.

The behaviour of these composites based on 2-dimensional nanofillers is even more complex when used in fibers and textiles, because the fiber diameter can be comparable to the size of the nanosheet. For this, we use for the first time a combination of macroscopic mechanical tests, microscopic characterization and numerical modelling to understand how the mesoscopic nanosheets are positioned into (or onto) the fibers, and how this influences the failure mechanism of the material at the nanoscale.

In these systems, the sheets can act as mechanical reinforcement of the fiber, but also as defects oriented perpendicular to the fiber axis, or can be segregated outside the fiber, thus having little effect on fiber properties. Including graphene in polymer sheets and in thin polymeric fibers is a major challenge for applications in e-textiles and bio-compatible electronics [34].

2. Experimental

2.1. Preparation of GO

Graphene oxide was prepared from graphite flakes by a modified Hummers method [17] and characterized before use by spin coating part of the solution on flat silicon wafers, and observing sheet size by Atomic Force Microscopy (AFM). As expected, the material was composed mainly by monoatomic sheets, with minimal amounts of thicker aggregates [17,18,35].

A 7.5 mg/mL GO solution in water was diluted 45 times before the characterization process. A Chemat technology spin-coater KW-4A was used for 60 s at 2000 rpm to spin-coat the GO solutions on SiO_2 films. The samples were spun in open air using 100 μL of the diluted GO solutions. Spin-coating was used to make a uniform distribution of GO sheets on the substrates.

2.2. Preparation of gelatin–GO films

Type A gelatin (280 Bloom, Italgelatine S.p.A.) from pig skin was used. Different amounts of a 7.5 mg/mL GO solution were added, under continuous stirring, to a 10% (w/V) aqueous gelatin solution at 40 °C, in order to obtain films containing gelatin and different GO amounts (0.5, 1, 1.5, 2% w/w) in the final composition. Films were obtained on the bottom of Petri dishes (diameter = 6 cm) after water evaporation at room temperature (RT) from 10 ml of solution.

The samples were labelled as F-0.5, F-1, F-1.5, F-2. Pure gelatin films were used as reference, and named F-0. Composite film containing a higher fraction of GO, 0.5 wt% gelatin and 0.5 wt% GO (Gel:GO = 1:1) was also produced, and labelled as G0.5GO0.5.

2.3. Preparation of gelatin–GO electrospun mats

Gelatin was dissolved in acetic acid/double distilled water 60/40 (v/v), at a concentration of 25% (w/v). The solution was stirred at 50 °C for 60 min, maintained under stirring overnight and then electrospun to obtain the control mat free of GO. Different amounts of a 7.5 mg/mL GO solution were added, under continuous stirring, to aqueous gelatin solution in acetic acid/ double distilled water 60/40 (v/v) at 50 °C, in order to obtain suspensions containing a gelatin concentration of 25% and a GO content of 0.5, 1 and 1.5% (wt%) in the final electrospun mat composition.

The electrospinning homemade apparatus was composed of a high voltage power supply (Spellman, SL 50 P 10/CE/230), a syringe pump (KD Scientific 200 series), a glass syringe, a stainless-steel blunt-ended needle (inner diameter: 0.84 mm) connected with a grounded rotating collector (length = 12 cm, diameter = 5 cm) positioned 15 cm away from the tip of the needle. The polymer solution was dispensed, through a Teflon tube, to the needle that was horizontally placed in front of the collecting mandrel. All the above described solutions were electrospun into non-woven mats by using the following conditions: applied voltage = 20 kV, needle to collector distance = 10 cm, solution flow rate = 0.005 ml/min, at RT and relative humidity, RH = 40 ÷ 50%. Fibers were collected with a random arrangement on the cylinder rotating at a speed of about 2 m/s. Electrospun mats were kept under vacuum over P_2O_5 at RT overnight in order to remove residual solvents. Gelatin electrospun mats were labelled as M-0 whereas gelatin–GO electrospun mats were labelled as M-0.5, M-1, M-1.5 according to GO content.

2.4. Morphological investigation

AFM measurements were carried out using an NT-MDT AFM in air operating in semi-contact (tapping) mode, using commercial Bruker n-doped Silicon (Si) AFM tips in a semi-contact (tapping) mode. In order to obtain quantitative results from the topographic AFM images of GO we used statistical image analysis software (Scanning Probe Image Processor, SPIP from Image Metrology and OriginPro 8.1 SR3). Morphological investigation of the composite samples was performed using a Philips XL-20 Scanning Electron Microscope (SEM). The samples were sputter-coated with gold prior to examination. The distribution of electrospun fiber diameters was determined through the measurement of about 150 fibers by means of an acquisition and image analysis software (EDAX Genesis) and the results were given as the average diameter ± standard deviation. Electrospun fibres supported on conventional copper microgrids were observed by using a Philips CM 100 Transmission Electron Microscope (TEM) operating at 80 kV.

2.5. Mechanical tests

Mechanical characterization was carried out on strip shaped (3 × 30 mm, thickness around 0.12 mm, determined by micrometer) samples obtained after film immersion in H_2O/Ethanol (2/3) solution for 10 min and on strip-shaped electrospun mats (5 mm × 20 mm, thickness ranging from 0.012 to 0.017 mm, determined by micrometer). Stress–strain curves were recorded on dried samples using an INSTRON Testing Machine 4465, and the Series IX software package. Crosshead speed was set at 5 mm/min in the case of films and at 0.5 mm/min for the electrospun mats. The Young's modulus E, the stress at break σ_b and the strain at break ε_b of the strips were measured in a static mode.

At least ten specimens were measured for each sample type and results were provided as the average value ± standard deviation.

2.6. Differential scanning calorimetry (DSC)

Calorimetric measurements were performed using a Perkin–Elmer Pyris Diamond DSC equipped with a model ULSP intracooler. Temperature and enthalpy calibration were performed using high-purity standards (n-decane and indium). The sample weights were in the range of 3–4 mg. Samples were examined in air-dried conditions. Heating was carried out at 5 °C/min from 40 °C to 150 °C. Denaturation temperature (T_D) was determined as the peak value of the corresponding endothermic event. The value of denaturation enthalpy was calculated with respect to the weight of air-dried gelatin.

2.7. Swelling

Square-shaped films (1 cm^2) were immersed in phosphate buffered solution (0.1 M, pH 7.4) for different periods of time. Wet samples were wiped with filter paper to remove excess liquid and weighted. The amount of adsorbed water was calculated as

$$W(\%) = 100\frac{(W_w - W_d)}{W_w}$$

Where W_w and W_d are the weights of the wet and the air dried samples, respectively.

2.8. X-ray diffraction (XRD) analysis

X-ray diffraction analysis was carried out by means of a Panalytical X'Celerator Powder diffractometer. CuKα radiation was used (40 mA, 40 kV). The 2θ range was from 3° to 50° with a step size of 0.033° and time/step of 20 s.

3. Results and discussion

In many cases, the main challenge in creating a composite material is to maximize the interaction between the two (or more) components of the material, to obtain a new product that merges together the beneficial properties of all the constituents. A scheme representing gelatin–GO composites preparation process is shown in Fig. 1. A major issue in
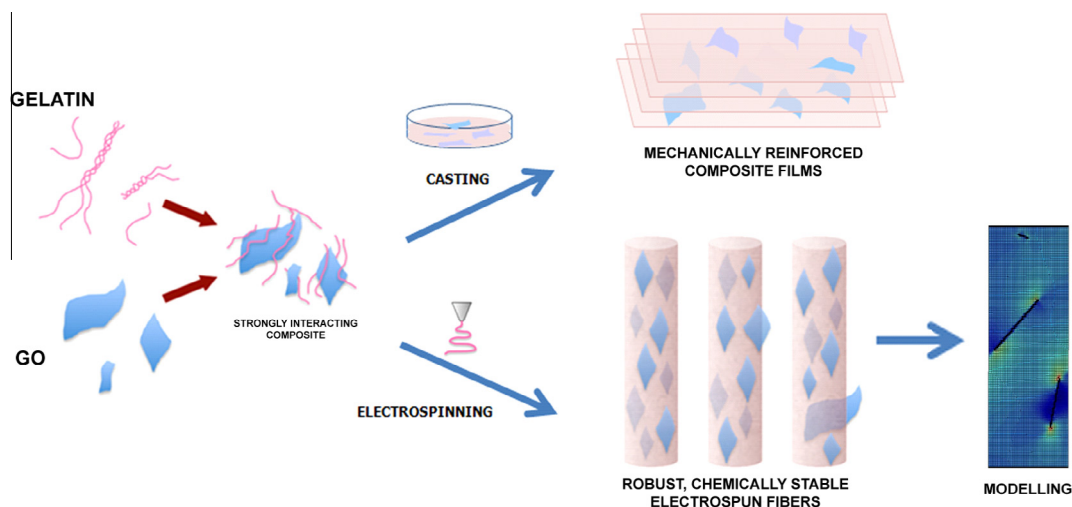
Fig. 1 – Scheme of gelatin–GO composites preparation process, and numerical modelling of the gelatin–GO nanofibres at the lowest hierarchical level. (A colour version of this figure can be viewed online.)

composites based on graphene and graphene oxide is the re-stacking of the sheets due to poor interaction with the polymeric matrix, which creates large defects in the composite, reduces the processability and requires higher loading of graphene to obtain a significant improvement of the properties of the material.

Interestingly, the composite materials described in this work display an excellent interaction between the two different components both in the shape of films and as co-electrospun nanofibers.

3.1. GO nanosheets

Fig. 2 reports the AFM image, thickness profile and statistical analysis of the GO nanosheets utilized for the preparation of the nanocomposites. Using image analysis, 2197 sheets in 4 different samples were measured. For each sheet, the length L and width W were calculated, as well as the aspect ratio L/W (Fig. 2c).

Given the irregular shape of the sheets, the definition of L and W is not unique. To avoid any ambiguity, we use as relevant parameter the square root of the area measured exactly for each sheet (pixel by pixel) by image analysis software: $S = \sqrt{A_{measured}}$, which has the same units of length and width. This value would correspond roughly, in the case of rectangular shapes, to the geometrical mean of the length and width. Instead, the irregular shape of the sheets gives in all cases $S \neq \sqrt{LW}$. Thus, while L and W are arbitrary axes chosen for each flake by the image analysis software, S is an objective value directly obtained for the flake area.

Statistical analysis for this solution yields $S = 84 \pm 66$ nm, $L = 113 \pm 98$ and $W = 56 \pm 44$ nm. This average must only be considered as indicative, because the size distribution does not follow a Gaussian (a.k.a. "normal") distribution, but it is strongly asymmetric and positively skewed, as typical in many poly-dispersed materials, like powders or polymer blends, giving a very high variance of the average. From the slope of the fitted line we calculated the aspect ratio of

length/width that is 3 ± 0.05. The average thickness of the sheets as measured by AFM on silicon was 1.1 ± 0.3 nm.

3.2. Gelatin–GO Films

Well dispersed gelatin–GO composite films were obtained using a simple assembling procedure as described in the Section 2. The good dispersion of GO inside the biopolymer is confirmed by the photographs of the films reported in Fig. 3, which show a homogeneous coloration. The intensity of the yellow/brown colour increases on increasing GO content of the composites. Some GO aggregates can be detected in F-1.5 and F-2.

Moreover, Scanning Electron Microscopy (SEM) images of the fractured film surfaces display a layered morphology, with the presence of GO sheets between the layers, as shown in Fig. 4 for F-0.5. The GO sheets (indicated by white arrows) appear embedded in between layers of biopolymer; although SEM does not allow the measurement of the thickness of the GO flakes, many of them appear very thin, with just occasionally some thicker platelets (an example is shown Fig. 4b). Overall, SEM data indicate a good dispersion of GO in the matrix, in agreement with XRD data (see below).

The DSC plots of dry composites exhibit an endothermic peak due to collagen denaturation, as a consequence of the helix-coil transition. The values of denaturation temperature, T_D, and enthalpy, ΔH_D, of the films at different GO content are reported in Table 1. Contrary to T_D values, which do not show significant variations as a function of composition, the values of ΔH_D decrease on increasing GO content. Since ΔH_D is related to the relative amount of triple helical structure in the samples, these data suggest that the presence of GO during gelling interferes with the renaturation process of gelatin and reduces the triple helix content of the composite films. This finding is supported by the results of X-ray diffraction analysis (Fig. 5). The XRD pattern of gelatin shows a reflection at about 8° of 2θ, corresponding to a periodicity of about 1.1 nm, which is associated to the diameter of the collagen
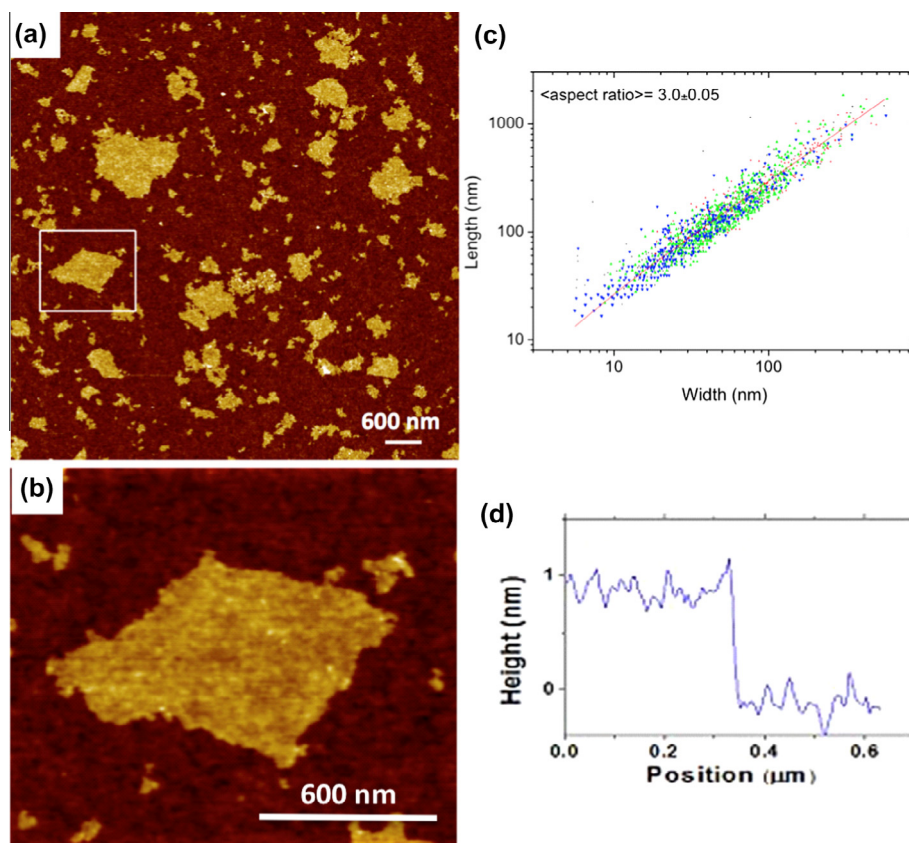
Fig. 2 – (a and b) AFM image of GO sheets spin coated on silicon. (c) Statistical analysis of the length/width ratio of the GO sheets, in log–log scale. The different colors of the points in the plot correspond to four different samples that were analyzed. (d) Height profile taken along the dashed line in (b). (A colour version of this figure can be viewed online.)
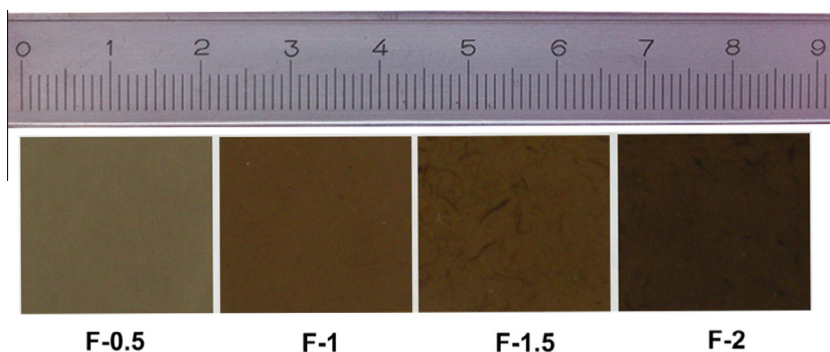

Fig. 3 – Photographs of the gelatin–GO composite films at different GO content: the intensity of the yellow/brown color increases on increasing GO content. The scale is in centimeters. (A colour version of this figure can be viewed online.)

triple helix, and a broad peak in the range 12–30° of 2θ related to peptide bonds. The integrated intensity of the first reflection can be used as a measure of the degree of renaturation, or triple-helix content, of gelatin films [7]. In particular, herein the relative amount of triple helices (X) within the samples has been determined by dividing the integrated intensity of this reflection by that of the broad peak associated to peptide bonds [36].

The comparison of the XRD patterns reported in Fig. 5 shows a decrease of the relative intensity of the 1.1 nm reflection on increasing GO content of the films. In agreement with this qualitative observation, the values of X decrease as well from 21% for F-0 to 18% for F-0.5, to 12% for the samples at greater GO content. The reduction of the triple helix content revealed by DSC and XRD results is similar to that observed on crosslinked gelatin, where the degree of renaturation of the protein decreases on increasing the degree of crosslinking [6,10]. It can be suggested that the interaction of the oxygen-rich groups on the GO surface with gelatin chains during gelling interferes with gelatin renaturation
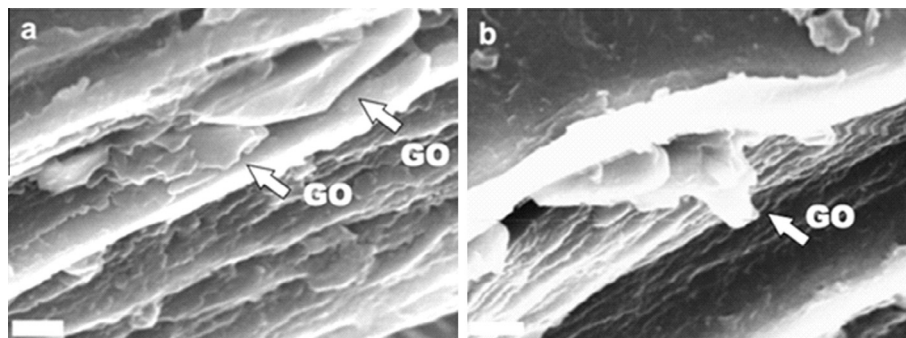
Fig. 4 – (a and b) Scanning electron microscopy of F-0.5 fractured surface: the arrows indicate the GO platelets which appear embedded in between the layers of gelatin. Scale bar: 5 μm.

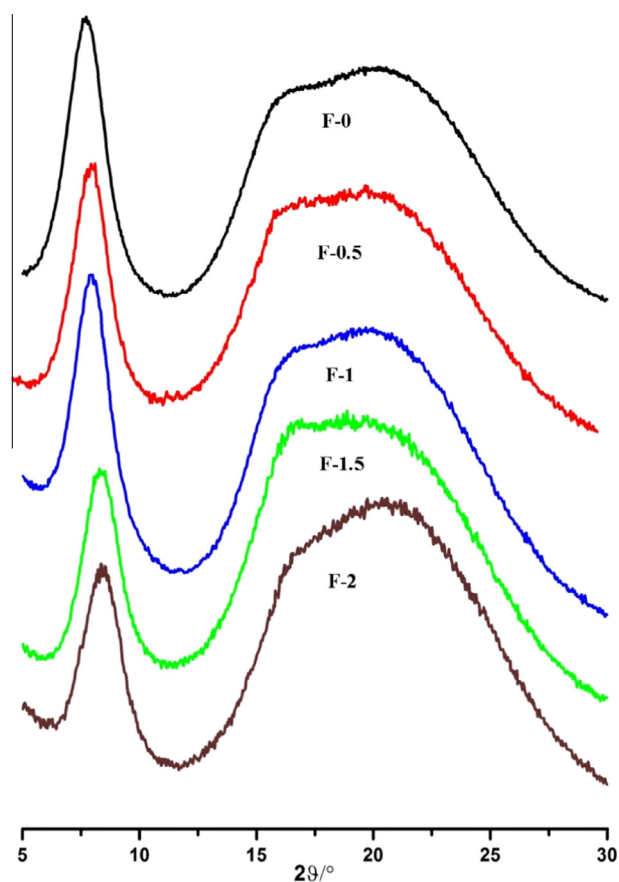| Table 1 – Denaturation temperature (T_D) and denaturation enthalpy (ΔH_D) of the endothermic peak event for gelatin–GO films.		
Sample	T (°C)	ΔH (J/g)
F-0	94 ± 1	32 ± 1
F-0.5	91 ± 1	29 ± 1
F-1	91 ± 1	29 ± 1
F-1.5	91 ± 1	28 ± 1
F-2	91 ± 1	26 ± 1

Fig. 5 – XRD diffraction patterns of gelatin-GO films: the amount of GO increases from the top spectrum to the bottom one. (A colour version of this figure can be viewed online.)
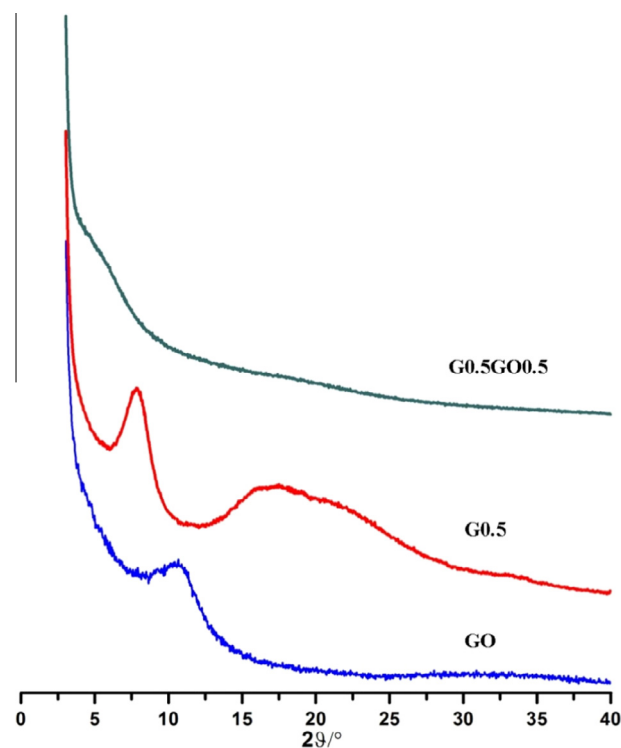

Fig. 6 – XRD diffraction patterns obtained from GO powder (GO), 0.5 wt% gelatin film (G0.5), and G0.5GO0.5 film. (A colour version of this figure can be viewed online.)

and reduces the extent of triple helix content, in agreement with previous studies [16]. The XRD pattern of GO displays a broad peak at about 10.8° of 2θ, corresponding to an interplanar distance of about 0.76 nm (Fig. 6). In contrast, the XRD patterns of gelatin/GO composite films do not exhibit any reflection due to GO, (Fig. 5), most likely because of the low GO content and/or due to the good exfoliation of GO sheets in the gelatin matrix [16,37]. In order to test this hypothesis, a few films at low gelatin concentration and at very high GO contents, up to 50 wt% have been prepared and characterized. The XRD patterns of these films display neither reflections due to gelatin nor to GO (Fig. 6), and their DSC plots do not show the presence of any endothermic peak (data not shown), confirming that GO and gelatin are interacting effectively in

Table 2 – Strain at break (ε_b), stress at break (σ_b), and Young's modulus (E) of gelatin–GO films. Each value is the mean of at least 10 determinations reported with the standard deviation.

Sample	σ (MPa)	E (GPa)	ε (%)
F-0	79 ± 9	2.1 ± 0.3	14 ± 4
F-0.5	86 ± 9	2.6 ± 0.2	18 ± 3
F-1	100 ± 4	3.1 ± 0.5	20 ± 3
F-1.5	107 ± 5	2.9 ± 0.2	24 ± 4
F-2	97 ± 5	2.9 ± 0.3	17 ± 3

Table 3 – Swelling (% wt) of gelatin–GO films as a function of storage time in physiological solution. Each value was determined in triplicate.

Sample	1 min	5 min	30 min	60 min	180 min	1 d	2 d	7 d	14 d
F-0	124 ± 4	253 ± 3	562 ± 4	714 ± 3	882 ± 4	998 ± 10	1470 ± 8	–	–
F-0.5	136 ± 8	264 ± 4	510 ± 3	611 ± 3	740 ± 4	960 ± 6	1200 ± 6	1416 ± 8	–
F-1	127 ± 5	240 ± 5	481 ± 5	607 ± 5	752 ± 5	971 ± 5	1040 ± 8	1280 ± 8	1692 ± 8
F-1.5	121 ± 3	236 ± 4	491 ± 4	600 ± 5	733 ± 6	880 ± 5	940 ± 5	1140 ± 5	1450 ± 8
F-2	117 ± 6	229 ± 5	491 ± 6	600 ± 4	744 ± 5	890 ± 6	920 ± 5	1040 ± 6	1200 ± 10

the composite, and that GO hinders the gelatin renaturation process. On the other hand, the absence in the XRD patterns of the GO peak at about 10.8° of 2θ and the presence of a shoulder at about 5.4° of 2θ confirms the tendency of GO to assume an intercalated structure within gelatin composites.

The mechanical properties of the composites improve on increasing GO content, in agreement with its reinforcement action on gelatin. Stress–strain curves recorded from air-dried samples were used to evaluate the Young's modulus, E, the stress at break, σ_b, and the deformation at break, ε_b, of the films. The results reported in Table 2 show that even a relatively low GO concentration (1 wt%) yields a remarkable increase of both E and σ_b, whereas a greater GO addition up

to 2% does not cause further improvement of the mechanical parameters. The reinforcement action of the filler also reduces the degree of swelling of the composite films, as seen from the data reported in Table 3. Gelatin is highly soluble and immersion in phosphate buffer induces considerable swelling,

which reaches about 900% in three hours. Gelatin films completely dissolve after 2 days. In agreement with the reinforcement action of GO, composite films display reduced swelling, F-0.5 resists up to 7 days and the dimensions of the samples richer in GO can still be measured after 2 weeks in phosphate buffer. The stabilizing action can be explained with both a mechanical reinforcement induced by GO and
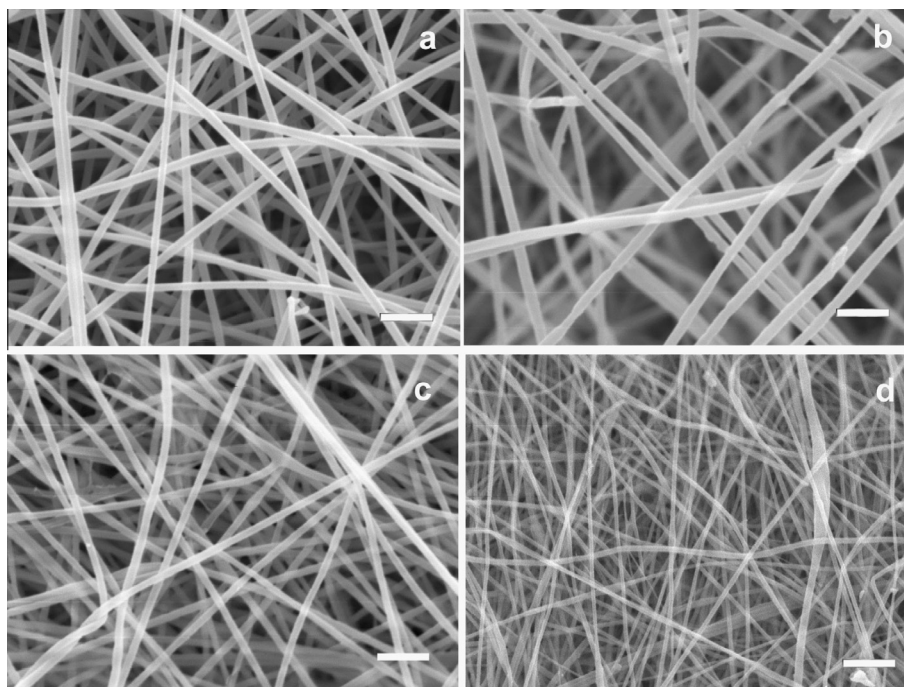
Fig. 7 – Scanning electron microscopy of electrospun gelatin–GO mats (a) M-0, (b) M-0.5, (c) M-1, (d) M-1.5. Scale bar: 5 μm.
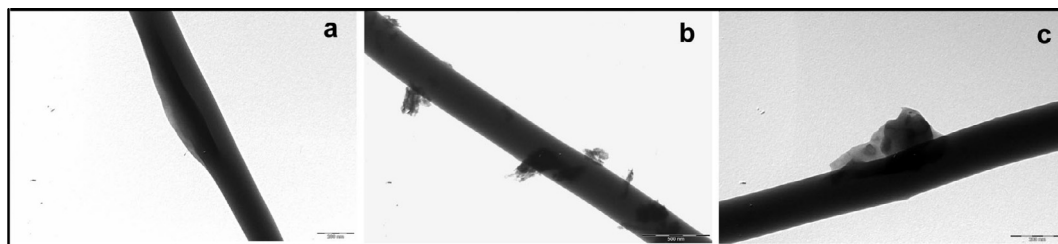
Fig. 8 – Trasmission electron microscopy of electrospun M-1 mat showing GO flakes deposited (b) on the surface or (a and c) partially embedded into gelatin fibers. Scale bar: 200 nm (a and c); 500 nm (b).

with a protective effect of the large, highly anisotropic 2-dimensional GO sheets that act as a barrier to water intake into the more open, 3D porous gelatin matrix.

3.3. Electrospun gelatin–GO fibers

In view of the similar properties exhibited by F-1.5 and F-2, the preparation and characterization of nanofibrous gelatin–GO mats were limited to graphene oxide contents up to 1.5 wt%. The mats of pure gelatin (M-0) display interconnected porosity and are made of randomly arranged fibers with smooth surface and a uniform mean diameter of about 270 nm (Fig. 7a). Therefore, electrospinning conditions used to produce the fibers (solution composition, experimental parameters and environmental parameters) have been successfully optimized to obtain fibers without bead defects along the fiber axes. The nanofibers are uniform in diameter and smooth in surface, with a mean diameter of about 270 nm. The preparation of the composite scaffolds is a very delicate assembly process since the dimensions of GO sheets are comparable to fibre diameters. Nonetheless, the presence of GO in the composite scaffolds does not seem to affect the smoothness and uniformity of the nanofibers (Fig. 7b–d), indicating a good performance of the optimized electrospinning conditions.

The main variation provoked by GO on fiber morphology is the reduction of the fiber mean diameter observed in the sample M-1.5, which displays a mean diameter of 150 ± 40 nm, in contrast to those of the other samples (270 ± 40 nm). Reduction of the diameter of electrospun fibers with GO content has been previously observed in different polymers and ascribed to the increase of conductivity of the electrospinning solution due to GO addition, which yields thinner fibers [30,38]. The increased conductivity has been explained in previous works as the GO reduction promoted by gelatin amino groups, which could be oxidized to nitrite [39]. The real process is likely due to a more complex combination of causes; GO is indeed known as an insulator [40], but the presence of GO sheets having size comparable to the fiber diameter will strongly influence the viscosity and dielectric constant of the solution, changing the response to the strong electric fields (20 kV) and to the mechanical stress applied during electro spinning (typical spinning speed is 2 m/s).

TEM images show the presence of GO flakes comparable in size to the fiber diameter, onto the gelatin nanofibers (Fig. 8b), whereas further images show GO nanosheets partially embedded in the nanofibers (Fig. 8a and c). While these large
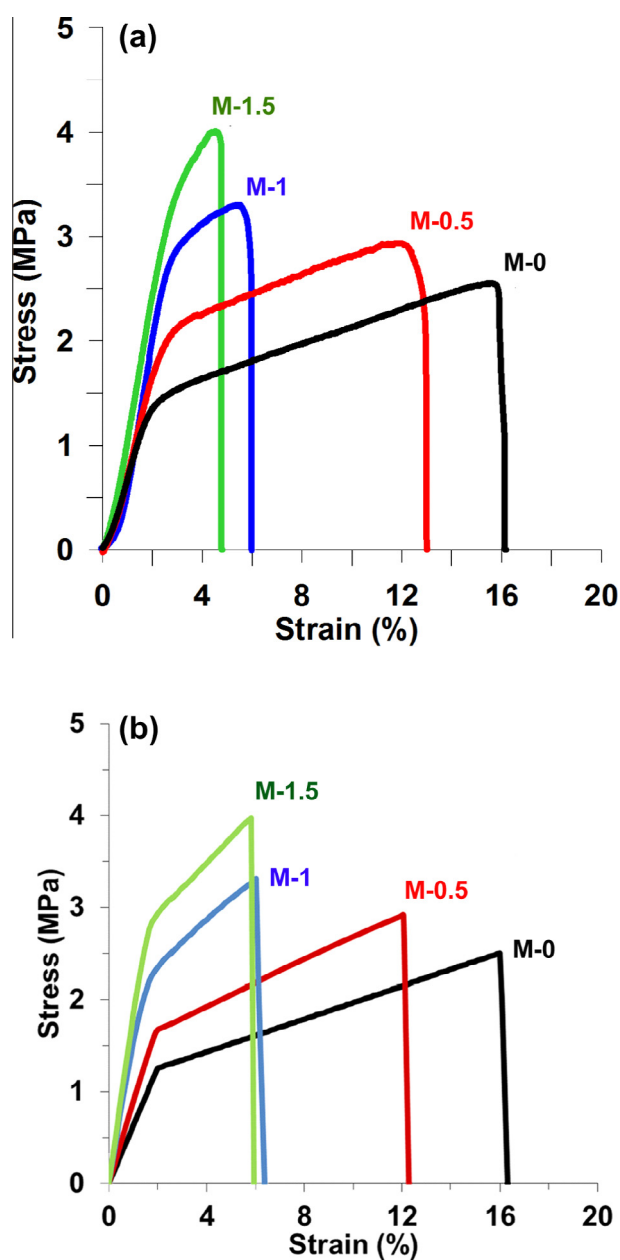

Fig. 9 – (a) Representative stress strain curves of gelatin–GO nanofiber mats as a function of the composition. (b) Corresponding numerically calculated Stress–Strain curves. (A colour version of this figure can be viewed online.)

flakes are clearly visible by TEM and can act as defects in the fiber, statistical analysis (Fig. 2c) shows that the majority of the flakes have a width smaller than fiber diameter (150 nm), and thus will be fully embedded into the fibers.

Representative stress–strain curves of gelatin–GO nanofibers are shown in Fig. 9a. The variation of the curves as a function of composition clearly shows that GO is also effective in reinforcing electrospun gelatin fibers, as previously observed for bulk films.

As for GO–gelatin films [16], all samples display elastoplastic behavior, and the increasing GO reinforcement content is responsible for an increase in the slope of both the elastic and plastic phases, and for a decrease in the ultimate strain values, leading to a reduction of the plastic phase for high reinforcement percentages. The values of the Young's modulus, E, the stress at break, σ_b, and the deformation at break, ε_b, of the scaffolds are reported in Table 4. The deformation at break decreases for increasing GO content, and it assumes minimum values for M-1 and M-1.5, which also display greater values of σ_b than pure gelatin mats. Moreover, these same samples exhibit an increase of the value of Young's modulus of about 50% with respect to that of pure gelatin mats. This increase can also be qualitatively predicted by a simple rule of mixtures calculation [41], however, due to the variable size, dimensions and orientations of reinforcements, a more refined numerical approach is required, and presented in Section 3.4 below.

3.4. Numerical simulations

To simulate the mechanical behaviour of the gelatin–GO nanofiber system, a numerical approach was used based on a previously developed Hierarchical Fibre Bundle Model [42], also employed for heterogeneous media [43,44] and graphene composites [45], and extended here to 2-D to account for shear effects. The simulations were implemented in a hierarchical scheme in two steps: (a) the GO-reinforced gelatin fibres were modelled at nanoscale using an in-house developed 2-D Finite-Element Model (FEM) formulation accounting for elastoplastic behaviour and fracture initiation and propagation, and (b) the electrospun mat geometry was modelled at micro/mesoscale using a fibre bundle model with input fibre properties (i.e. yield and fracture stresses and strains) determined from the nanoscale FEM simulations. More specifically:

a) For the FEM simulations, representative portions of the gelatin fibres containing various GO reinforcements were discretized in a 2-D quadrilateral-element mesh, as shown in Fig. 10a: each element consists of $i = 4$

nodes, each with two degrees of freedom (u_i and v_i), with 6 inter-nodal relationships in the element. A typical mesh contains about 10^4 square elements, corresponding to approximately 2×10^4 degrees of freedom (accounting for common nodes between adjacent elements), with each element corresponding to an area of approximately 4.5 by 4.5 nm^2. The GO flakes are modelled with randomly varying orientation and dimensions corresponding to those reported in Fig. 2c, so as to obtain an average length of about 110 nm and width of about 50 nm. The constitutive relation for the matrix is elasto-plastic and derived directly from experimental data (specimen M-0, Fig. 9a). We used for the simulation an effective Young's modulus $E_{m,e} = 62.5$ MPa, calculated from the linear part of the stress–strain M-0 curve in Fig. 9a, to account for softening effects always present before the yield point. We also used as yield strain $\varepsilon_{m,e} = 2\%$, an elastic modulus (in the plastic region) $E_{m,p} = 8.9$ MPa, and fracture strain $\varepsilon_{m,p} = 16\%$. A perfect interface was considered between the reinforcements and the matrix, and possible failure mode are platelet/matrix debonding as well as crack propagation in the matrix. Due to the thickness of about 1 nm of the GO flakes and the larger discretization size used in the mesh to optimize computational times, for the reinforcements it was necessary to model representative GO–gelatin portions, with GO flakes constituting about 1/5th of the considered 10 nm thickness. The corresponding Young's modulus E_r was derived from the GO modulus $E_{GO} = 200$ GPa [46] using a rule of mixtures, thus obtaining $E_r = 1/5 \cdot E_{GO} + 4/5 \cdot E_{m,e} = 40$ GPa. The validity of this approximation was checked and found to be responsible for only a small variation in the results (10% at most in the fracture stress). The GO flakes were assumed to be randomly oriented and randomly positioned in the matrix, with statistical variation in the size as derived from experimental data (see Fig. 2c). Due to the variation of these parameters, simulation results are statistically distributed and simulations are repeated various times to obtain the corresponding distributions in output parameters.

b) Regarding the FBM simulations, the electrospun gelating mats shown in Fig. 7 were modelled as networks of fibres arranged in parallel and in series subjected to uniaxial tension, with statistically-distributed yield and fracture strengths, according to the input parameters from FEM simulations. We adopted an equivalent load sharing hypothesis [42], whereby when fibres fracture, stresses are redistributed uniformly among the

Table 4 – Strain at break (ε_b), stress at break (σ_b), and Young's modulus (E) of gelatin–GO mats. Each value is the mean of at least 10 measurements reported with the standard deviation.

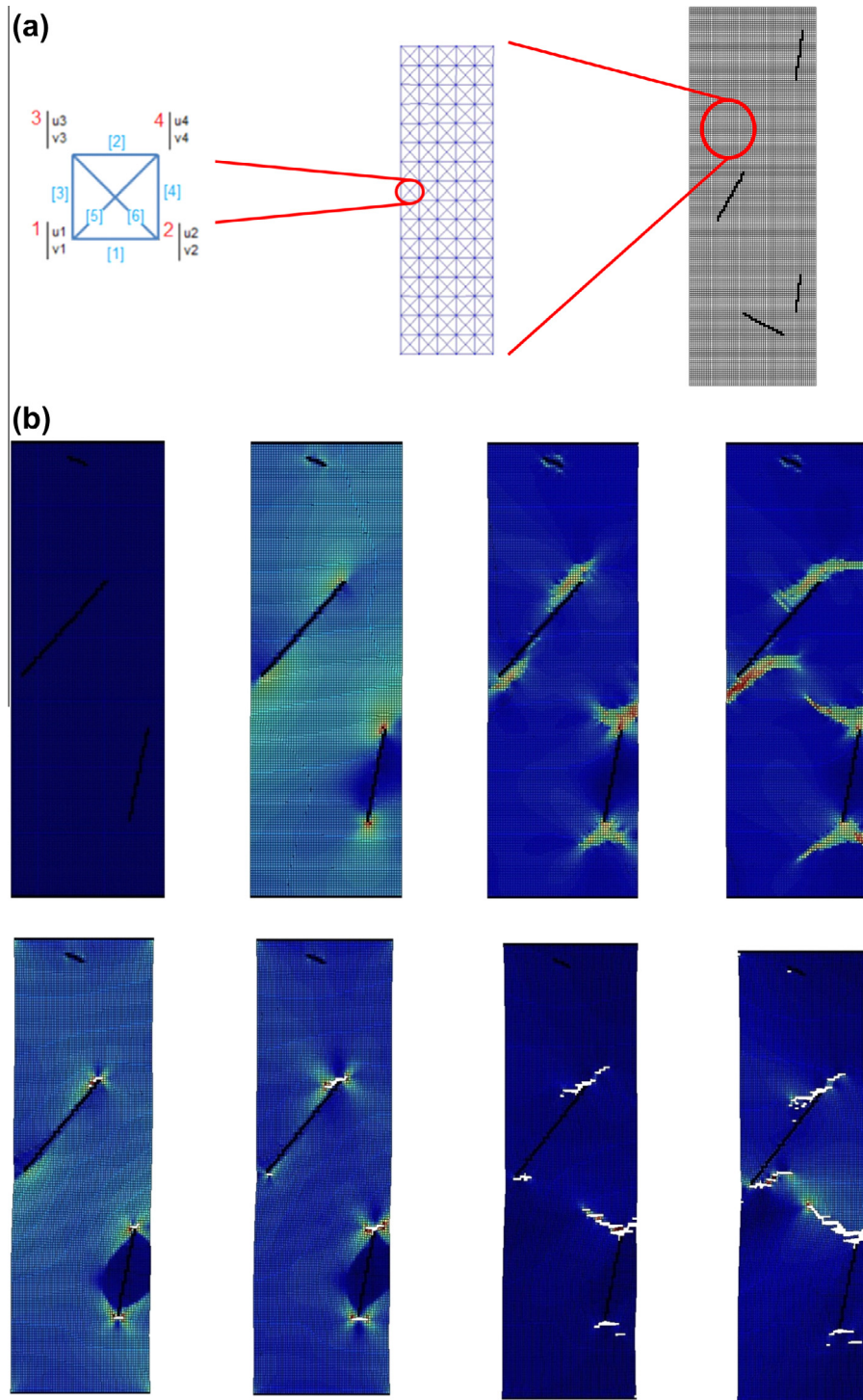| Sample	σ (MPa)	E (MPa)	ε (%)
M-0	2.5 ± 0.6	90 ± 20	17 ± 2
M-0.5	2.9 ± 0.6	92 ± 18	12 ± 2
M-1	3.4 ± 0.5	148 ± 9	5.4 ± 0.7
M-1.5	4.1 ± 0.4	141 ± 1	5 ± 1

Fig. 10 – (a) Schematic of the quadrilateral elements used in the model and FEM mesh of a typical GO-gelatin nanofibre specimen. Nodal degrees of freedom (u_i,v_i) are also indicated; (b) development of crack propagation leading to nanofibre failure at the lowest size scale considered numerically. Successive images show stress concentrations leading first to failure in isolated areas, and finally in the whole specimen. (A colour version of this figure can be viewed online.)

remaining fibres in the same bundle section. Specimen dimensions were 5 mm in width, 30 mm in length, and 0.08 mm in thickness, which given the measured 91% mat porosity, 270 nm fibre diameter and assumed mean fibre length of 0.1 mm, correspond to fibre bundles of approximately 10^3 fibres in parallel. Mechanical properties of the fibres were derived from FEM simulations. In FBM calculations, the specimens were subjected to

tensile loading up to failure in repeated tests to derive the corresponding macroscopic stress–strain behaviour, accounting for statistical variation, and results were compared to experimental data.

FEM simulations show that cracks develop at nanoscale in the regions at the tips of reinforcements due to stress concentrations, but their propagation is partially neutralized by the matrix nonlinear behaviour, which concentrates deformations and failure at the initial site of the crack, thus limiting further propagation. This type of behaviour, which is shown in Fig. 10, is consistent with predictions in the literature [47].

The resulting stress–strain curves for the different considered percentages of GO reinforcements in the matrix (M0.5, M1, M1.5) are shown in Fig. 9b. A considerable agreement is obtained with experimental curves (Fig. 9a), with only a slight discrepancy in the fracture strain for the M1.5 sample Overall, simulations capture an increase of the elastic modulus both before and after the yield point for increasing GO percentages, as well as the yield stress increase. At the same time, simulations show that the GO–gelatin composite becomes more brittle with increasing GO content, so that fracture strain decreases.

4. Conclusions

The composite materials described in this work display an excellent interaction between the two different components; by mixing them together, both the renaturation of gelatin and the re-stacking of the GO sheets over each other are hindered, allowing a good mixing of the two phases. This effective interaction is even more remarkable because the building blocks of the composites have a very different nature; on the one hand we have highly polar and mechanically poor gelatin chains; on the other, we have 2-dimensional GO sheets, composed by large areas of apolar, sp^2-hybridized carbon mixed with more polar patches of sp^3-hybridized carbon, functionalized with hydroxyl, carboxyl and epoxy groups [40,48]. The two materials have different chemical composition, shape, size and origin.

Besides XRD, DSC, SEM and TEM evidence, the successful interaction of these two materials is demonstrated by the possibility to process them not only into films, but also into nanofibers by electrospinning, a quite demanding process that applies strong electrical and mechanical forces to the material. The gelatin–GO fibers are not only produced with good yield and uniformity, but also display higher Young's modulus and stress at break as compared to pure gelatin, albeit with a smaller diameter (150 nm vs. 270 nm).

This strong interaction can be ascribed to the good quality and high hydrophilicity of the adopted GO; and the modified Hummers method applied here [17] allows to have extremely soluble sheets, which show little tendency to re-stack even when deposited on surfaces at high concentrations [18]. Under stress, cracks develop eventually at nanoscale in the regions at the tips of reinforcements, but their propagation is partially neutralized by the matrix nonlinear behaviour, which concentrates deformations and failure at the initial site of the crack, thus limiting further propagation.

While the deposition of graphene or GO sheets on flat substrates is straightforward, their incorporation into more complex, nanostructured materials is still a challenge. The results presented here demonstrate that this issue can be overcome by using suitable chemically modified graphene and appropriate techniques, and that, because of the strong interaction, high processability, and huge aspect ratio, GO can be an ideal reinforcement for bio-materials such as these gelatin fiber networks.

REFERENCES

[1] Ruiz-Hitzky E, Aranda P, Darder M, Ogawa M. Hybrid and biohybrid silicate based materials: molecular vs. block-assembling bottom–up processes. Chem Soc Rev 2011;40:801–28.

[2] Yu G, Jialiang W, Zixing S, Jie Y. Gelatin-assisted fabrication of water-dispersible graphene and its inorganic analogues. J Mater Chem 2012;22:17619–24.

[3] Nicolosi V, Chhowalla M, Kanatzidis MG, Strano MS, Coleman JN. Liquid exfoliation of layered materials. Science 2013;340:1420.

[4] Pezron I, Djabourov M, Bosio L, Leblond J. X-ray diffraction of gelatin fibers in the dry and swollen states. J Polym Sci, Part B: Polym Phys 1990;28:1823–39.

[5] Gornall JL, Terentjev EM. Helix–coil transition of gelatin: helical morphology and stability. Soft Matter 2008;4:544–9.

[6] Boanini E, Rubini K, Panzavolta S, Bigi A. Chemico-physical characterization of gelatin films modified with oxidized alginate. Acta Bio 2010;6:383–8.

[7] Bigi A, Panzavolta S, Rubini K. Relationship between triple helix content and mechanical properties of gelatin films. Biomaterials 2004;25:5675–80.

[8] Yakimets I, Wellner N, Smith AC, et al. Mechanical properties with respect to water content of gelatin films in glassy state. Polymer 2005;46:12577–85.

[9] Zhang YZ, Venugopal J, Huang ZM, et al. Crosslinking of the electrospun gelatine nanofibers. Polymer 2006;47:2911–7.

[10] Bigi A, Cojazzi G, Panzavolta S, Roveri N, Rubini K. Stabilization of gelatin films by crosslinking with genipin. Biomaterials 2002;23:4827–32.

[11] Mano JF, Silva GA, Azevedo HS, et al. Natural origin biodegradable systems in tissue engineering and regenerative medicine: present status and some moving trends. J R Soc Interface 2007;4:999–1030.

[12] Bergo P, Sobral PJA. Effects of plasticizer on physical properties of pigskin gelatin films. Food Hydrocolloids 2007;21:1285–9.

[13] Wang W, Wang Z, Liu Y, et al. Preparation of reduced graphene oxide/gelatin composite films with reinforced mechanical strength. Mater Res Bull 2012;47:2245–51.

[14] Zheng J, Gao S, Li H, et al. Effects of reaction conditions on intercalation between gelatin and montmorillonite: thermodynamical impact. J Appl Polym Sci 2013;128:54–9.

[15] Bigi A, Panzavolta S, Roveri N. Hydroxyapatite–gelatin films: a structural and mechanical characterization. Biomaterials 1998;19:739–44.

[16] Wan C, Frydrych M, Chen B. Strong and bioactive gelatin–graphene oxide nanocomposites. Soft Matter 2011;7:6159–61.

[17] Treossi E, Melucci M, Liscio A, Gazzano M, Samorì P, Palermo V. High-contrast visualization of graphene oxide on dye-sensitized glass, quartz, and silicon by fluorescence quenching. J Am Chem Soc 2009;131:15576–7.

[18] Liscio A, Veronese GP, Treossi E, Suriano F, Rossella F, Bellani V, et al. Charge transport in graphene–polythiophene blends as studied by Kelvin Probe Force Microscopy and transistor characterization. J Mater Chem 2011;21:2924–31.

[19] Melucci M, Durso M, Zambianchi M, Treossi E, Zia ZY, Manet I, et al. Graphene–organic hybrids as processable, tunable platforms for pH-dependent photoemission, obtained by a new modular approach. J Mater Chem 2012;22:18237–43.

[20] Melucci M, Treossi E, Ortolani L, Giambastiani G, Morandi V, Klar P, et al. Facile covalent functionalization of graphene oxide using microwaves: bottom-up development of functional graphitic materials. J Mater Chem 2010;20:9052–60.

[21] Park S, Ruoff RS. Chemical methods for the production of graphenes. Nat Nanotechnol 2009;4:217–24.

[22] Cano M, Khan U, Sainsbury T, O'Neill A, Wang Z, McGovern IT, et al. Improving the mechanical properties of graphene oxide based materials by covalent attachment of polymer chains. Carbon 2013;52:363–71.

[23] Bortz DR, Heras EG, Martin-Gullon I. Impressive fatigue life and fracture toughness improvements in graphene oxide/epoxy composites. Macromolecules 2012;45:238–45.

[24] Shin MK, Lee B, Kim L, Lee JA, Spinks GM, Gambhir S, et al. Synergistic toughening of composite fibres by self-alignment of reduced graphene oxide and carbon nanotubes. Nat Commun 2012;3:650–5.

[25] Young RJ, Kinloch IA, Gong L, Novoselovb KS. The mechanics of graphene nanocomposites: a review. Compos Sci Technol 2012;72:1459–76.

[26] Zucchelli A, Focarete ML, Gualandi C, Ramakrishna K. Electrospun nanofibers for enhancing structural performance of composite materials. Polym Adv Technol 2011;22:339–49.

[27] Agarwal S, Wendorff JH, Greinier A. Use of electrospinning technique for biomedical applications. Polymer 2008;49:5603–21.

[28] Bao Q, Zhang H, Yang JX, et al. Graphene-polymer nanofiber membrane for ultrafast photonics. Adv Funct Mater 2010;20:782–91.

[29] Wang C, Li Y, Ding G, et al. Preparation and characterization of graphene oxide/poly(vinyl alcohol) composite nanofibers via electrospinning. J Appl Polym Sci 2013;127:3026–32.

[30] Papkov D, Goponenko A, Compton OC, An Z, Moravsky A, Li XZ, et al. Improved graphitic structure of continuous carbon nanofibers via graphene oxide templating. Adv Funct Mater 2013. http://dx.doi.org/10.1002/adfm.201300653.

[31] Wang Q, Du Y, Feng Q, et al. Nanostructures and surface nanomechanical properties of polyacrylonitrile/graphene oxide composite nanofibers by electrospinning. J Appl Polym Sci 2013;128:1152–7.

[32] Matsumoto H, Imaizumi S, Konosu Y, Ashizawa M, Minagawa M, Tanioka A, et al. Electrospun composite nanofiber yarns containing oriented graphene nanoribbons. ACS Appl Mater Interfaces 2013;5:6225–31.

[33] Pant HR, Park CH, Tijing LD, Amarjargal A, Lee DH, Kim CS. Bimodal fiber diameter distributed graphene oxide/nylon-6 composite nanofibrous mats via electrospinning. Colloids Surf A 2012;407:121–5.

[34] Yun YJ, Hong WG, Kim WJ, Jun Y, Kim BH. A novel method for applying reduced graphene oxide directly to electronic textiles from yarns to fabrics. Adv Mater 2013;25(40):5701–5.

[35] Perrozzi F, Prezioso S, Donarelli M, Bisti F, De Marco P, Santucci S, et al. Use of optical contrast to estimate the degree of reduction of graphene oxide. J Phys Chem C 2013;117:620–5.

[36] Zaupa A, Neffe AT, Pierce BF, Nochel U, Lendlein A. Influence of tyrosine-derived moieties and drying conditions on the formation of helices in gelatin. Biomacromolecules 2011;12:75–81.

[37] Yang XM, Tu YF, Li L, Shang SM, Tao XM. Well-dispersed chitosan/grapheneoxide nanocomposites. ACS Appl Mater Interfaces 2010;2:1707–13.

[38] Qi YY, Tai ZX, Sun DF, et al. Fabrication and characterization of poly(vinyl alcohol)/graphene oxide nanofibrous biocomposite scaffolds. J Appl Polym Sci 2013;127:1885–94.

[39] Liu K, Zhang JJ, Cheng FF, et al. Green and facile synthesis of highly biocompatible graphene nanosheets and its application for cellular imaging and drug delivery. J Mater Chem 2011;21:12034–40.

[40] Mattevi C, Eda G, Agnoli S, Miller S, Mkhoyan KA, Celik O, et al. Evolution of electrical, chemical, and structural properties of transparent and conducting chemically derived graphene thin films. Adv Funct Mat 2009;19:2577–83.

[41] Reddy JN. Mechanics of Laminated Composite Plates and Shells: Theory and Analysis 2nd ed. CRC Press; 2004.

[42] Pugno N, Bosia F, Carpinteri A. Multiscale stochastic simulations for tensile testing of nanotube-based macroscopic cables. Small 2008;4:1044–52.

[43] Bosia F, Abdalrahman T, Pugno N. Investigating the role of hierarchy on the strength of composite materials: evidence of a crucial synergy between hierarchy and material mixing. Nanoscale 2012;4:1200–7.

[44] Pugno N, Bosia F, Abdalrahman T. Hierarchical fibre bundle model to investigate the complex architectures of biological materials. Phys Rev 2012;E85:1080–3.

[45] Bosia F, Pugno N. In silico tensile tests of graphene fibres. Phys Status Solidi B 2013;250:1492–5.

[46] Gao Y, Liu LQ, Zu SZ, Peng K, Zhou D, Han BH, et al. The effect of interlayer adhesion on the mechanical behaviors of macroscopic graphene oxide papers. ACS Nano 2011;5:2134–41.

[47] Gao H, Ji B, Jäger IL, Arzt E, Fratzl P. Materials become insensitive to flaws at nanoscale: Lessons from nature. PNAS 2003;100(10):5597–600.

[48] Erickson K, Erni R, Lee Z, Alem N, Gannett W, Zettl A. Determination of the local chemical structure of graphene oxide and reduced graphene oxide. Adv Mater 2010;22:4467–72.